Influence of localization on the optical properties of ordered $(Al_{0.5}Ga_{0.5})_{0.52}In_{0.48}P$

U. Dörr, R. Lutz, E. Tsitsishvili,* and H. Kalt
Institut für Angewandte Physik, Universität Karlsruhe, D–76128 Karlsruhe, Germany
(Received 23 March 2000; revised manuscript received 25 July 2000)

Using various methods of optical spectroscopy, we have investigated the influence of localization on the optical properties of $CuPt_B$-type ordered $(Al_{0.5}Ga_{0.5})_{0.52}In_{0.48}P$. Localization results from the formation of inhomogeneous domainlike microstructures during the growth of the ordered material. We compare different samples which were grown simultaneously, but on differently oriented GaAs substrates. The samples exhibit completely different microstructures which were investigated in great detail by transmission electron microscopy and x-ray measurements. Typical localization effects like inhomogeneous broadening of the photoluminescence and the Stokes shift between photoluminescence and absorption are very pronounced if the structural correlation length is comparable to the exciton Bohr radius. In this case we have found two different types of localized states, i.e., one type at higher energies close to the band edge, and one at lower energies well below the band gap. The latter is attributed to anisotropic localization centers which are not significantly influenced by $CuPt_B$-type ordering. These centers produce modifications of the ordering-induced anisotropy of the photoluminescence. This phenomenon yields the possibility to obtain the mobility edge energy from the spectral dependence of the optical anisotropy. In temperature-dependent experiments, we have identified thermally activated exciton redistribution processes both within the localized states and from localized to extended states. If the excitation intensity is increased, state-filling effects produce a blue shift of the emission (moving emission). Using microphotoluminescence we demonstrate that this blueshift is not caused by a shift of single states but only by a change of their spectral weights. For high-excitation intensities above 10 kW/cm^2, we have identified global state filling which results in stimulated emission.

I. INTRODUCTION

Exciton localization in disordered semiconductors is a widely studied phenomenon which influences the optical properties of these material systems significantly. Most studies focus on two model systems: (a) mixed crystals with alloy disorder; and (b) quantum-well systems with well width fluctuations and, in some cases, additional alloy disorder. The reason for localization in such disordered systems is the existence of a fluctuating potential. In the case of alloy disorder, these fluctuations are produced by spatial variations of the band gap. In quantum-well systems, fluctuations of the well width and hence the quantization energy provide an additional source of potential variations.

At low temperatures, excitons are localized in local potential minima. The efficiency of this localization process depends on the ratio between the correlation length of the fluctuating potential, i.e., the ''size'' of the potential minima, and the excitonic Bohr radius, i.e., the ''size'' of the exciton.[1–4] For example, if the Bohr radius is significantly larger than the correlation length, localization is partly counterbalanced by averaging over many potential minima.

Although rarely discussed in this context, the quaternary semiconductor alloy $(Al_xGa_{1-x})_{0.52}In_{0.48}P$ is very suitable for an investigation of localization effects. In the disordered phase, i.e., for a completely random distribution of the group-III atoms (cations) on their sublattice, this material exhibits localization as a consequence of alloy disorder. However, since the excitonic Bohr radius in III-V compounds is very large in comparison to the correlation length, which is of the order of a few lattice constants, localization effects are not very pronounced in disordered $(Al_xGa_{1-x})_{0.52}In_{0.48}P$.

Depending on the growth conditions, the randomness of the distribution of the cations can be violated and the material acquires an ordered phase.[5] The most important type of ordered phase is the so-called $CuPt_B$-type ordering. In a $CuPt_B$-type ordered structure, the cation planes alternate as Al/Ga and In rich, approximating a monolayer superlattice along the $[1\bar{1}1]$ (variant I) or $[\bar{1}11]$ (variant II) directions.[6–8]

As a consequence of this ordering-induced symmetry reduction, the fourfold degenerate Γ_8^V valence-band state of the zinc-blende crystal (i.e., the disordered phase) splits into two twofold degenerate states of symmetry $\Gamma_{4,5}^V$ and Γ_6^V, respectively.[9,10] Since the matrix elements for optical transitions depend on light polarization, the ordered material exhibits optical anisotropy.[9–11]

With respect to localization, we have to take into account that real crystals are not homogeneously ordered, but exhibit domainlike microstructures with antiphase boundaries (APB's). While the actual morphology depends on all growth parameters, the substrate orientation is of particular importance since it is decisive for variant selection.[12–14] The inhomogeneity of the microstructure can be considered as *ordering-induced disorder* which involves potential fluctuations. We consider the size of the ordered domains as a measure for the correlation length of these fluctuations. Typical domain sizes range from a few nanometers to several micrometers,[15] and, hence, the correlation length is generally larger than in disordered crystals. As a consequence, ordered $(Al_xGa_{1-x})_{0.52}In_{0.48}P$ exhibits pronounced localization effects.

0163-1829/2000/62(23)/15745(9)/$15.00 PRB 62 ©2000 The American Physical Society

Localization in ordered $Ga_{0.52}In_{0.48}P$ or $(Al_xGa_{1-x})_{0.52}In_{0.48}P$ manifests itself as an inhomogeneously broadened emission band which occurs energetically below the absorption resonance, and exhibits several characteristic properties such as a blueshift with increasing excitation intensity and very long decay times.[16] In spatially resolved experiments it has been found that the low-energy emission is at least partly composed of very narrow lines which correspond to single excitonic states.[17]

These localized states have often been correlated to the APB's,[18,19] but Smith *et al.*[15] found that APB's cannot be the only origin of the typical low-energy emission. Obviously, localization and thus the properties of the low-energy emission strongly depend on the actual type of microstructure which can be identified in detail by transmission electron microscopy (TEM) and x-ray-diffraction methods.

In the present work we compare structural and optical investigations of different $(Al_{0.5}Ga_{0.5})_{0.52}In_{0.48}P$ samples which have been grown simultaneously. Since the substrate orientations are different, the samples exhibit completely different microstructures. The microstructures had been identified in great detail by TEM (Ref. 20) and x-ray-diffraction methods, and the correlation between structural peculiarities and localization effects is discussed. Using a large variety of spectroscopy methods we show that the optical properties are characterized to a very high extent by localization. In particular, localization modifies the ordering-induced anisotropy.

This paper is organized as follows. In Sec. II the microstructures of the samples are presented. Since structural inhomogeneities occur on a length scale of a few nanometers, the term *microstructure* is replaced by *nanostructure* in what follows. The different optical methods which have been applied are the subject of Sec. III. In Sec. IV we compare two $(Al_{0.5}Ga_{0.5})_{0.52}In_{0.48}P$ layers with different nanostructures with respect to the significance of typical localization effects. As a consequence of the particular type of nanostructure one sample exhibits pronounced localization effects. For this sample the ordering-induced optical anisotropy is affected by localization, and exhibits a typical spectral dependence. This is the subject of Sec. V. Since the absolute number of localized states is always small compared to the extended states, state filling plays an important role in localized systems, even for relatively low excitation intensities. In Sec. VI we compare state-filling effects in different regimes of excitation intensity. State filling results in population inversion and, consequently, stimulated emission. The paper is summarized in Sec. VII.

II. NANOSTRUCTURE OF THE SAMPLES

We have investigated $(Al_xGa_{1-x})_{0.52}In_{0.48}P$ layers which were grown under different conditions. In the following we concentrate on two different samples which are typical for different regimes of correlation length. The nanostructure of these samples has been determined in great detail. The two layers have a thickness of 1.5 μm, and were grown simultaneously in a horizontal atmospheric pressure metal-organic vapor-phase-epitaxy reactor on differently oriented substrates.[21] The growth temperature, growth rate, and V/III flow ratio were 700 °C, 2.5 μ/h, and $\sim$40, respectively. The

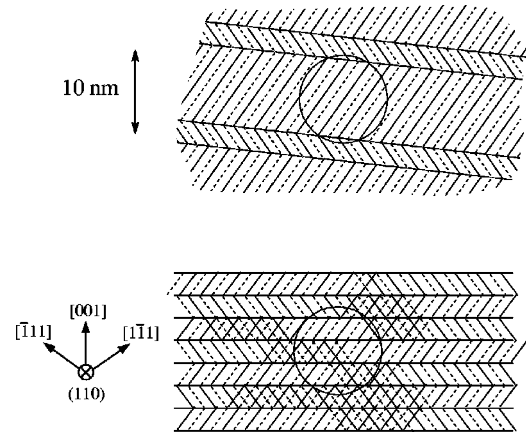

FIG. 1. Schematical representation of the nanostructures of the *l* sample (above) and the *s* sample (below). The In (Al/Ga) planes are represented as solid (dashed) lines. The circles indicate the size of an exciton.

sample with a very short correlation length (*s* sample) was grown on a GaAs(001) substrate misoriented by 10° toward {111}A. This sample therefore contains both ordering variants with equal volume fractions. In contrast, the substrate of the sample with a larger correlation length (*l* sample) is misoriented by 3° toward {111}B, and thus one ordering variant is preferred.

Using conventional and high resolution transmission electron microscopy, we identified the morphology of the samples down to a length scale of a few nanometers.[20] Since the details of the identified nanostructures and the respective experiments are described in Ref. 20, only a short summary of the experimental findings shall be given here. While the nanostructure of the *s* sample is characterized by very small domains containing each ordering variant, the *l* sample exhibits a nearly regular succession of platelike domains. The suppressed variant occurs in 1–2-nm thin domains which separate the more extended domains of the preferred variant, and form antiphase boundaries between them. The domains of the preferred variant have a thickness of $\sim$10 nm. While this value is comparable to the excitonic Bohr radius of the material, the structural correlation length of the *s* sample is found to be 1–2 nm, and thus much smaller than the excitonic Bohr radius. This is illustrated in Fig. 1, where the nanostructures of the samples are depicted schematically.

Since exciton localization in inhomogenous structures depends strongly on the ratio between the length scale of the potential fluctuations and the excitonic Bohr radius, the different structural correlation lengths of the two samples result in a different significance of localization effects. This is described in detail in Sec. IV. In Sec. III we first present some details of the optical experiments.

III. EXPERIMENTAL METHODS

Polarized, spatially integrated measurements of the photoluminescence (PL) were carried out using the 514.5-nm line of an Ar^+ laser as the excitation source. In order to avoid errors produced by any polarization dependence of the detection system, a polarization filter was placed in the detection beam. The detected polarization was selected using a

double fresnel rhomb. As detection system we have used a combination of a 64-cm grating spectrometer and a diode array. The spectral resolution was ~1 meV. In order to control the sample temperature between 5 and 300 K, a helium bath cryostat with integrated heating was used.

Spatial restricted measurements of the photoluminescence (μ-PL) were performed using a microscope objective in the detection beam. Spatial restriction of the detection spot was realized by a pinhole in the intermediate image plane of the microscope. With this setup a spatial resolution better than 1 μm was achieved.[22] A cooled charge-coupled-device (CCD) camera with a 75-cm grating spectrometer was used as detection system. The spectral resolution of this system was better than 80 μeV. A temperature control between 5 and 100 K was achieved using a helium flow cryostat.

For the high excitation experiments we used the pulses of a dye laser (Coumarin 153) pumped by a frequency tripled Nd:YAG (yttrium aluminum garnet) laser. The pulse duration was 3–4 ns, and the excitation wavelength 520–530 nm. Intensities of up to several MW/cm^2 were achievable with this setup. The high-excitation PL was measured in backscattering geometry using the same detection system as in the case of the spatially integrated PL.

IV. INFLUENCE OF THE NANOSTRUCTURE ON THE SIGNIFICANCE OF LOCALIZATION EFFECTS

As a consequence of localization the PL spectra of disordered materials exhibit a characteristic dependence on lattice temperature. In particular, the thermally activated redistribution of excitons within the tail of localized states manifests itself as a nonmonotonic dependence of the PL peak energy on temperature.[23–26] Starting from low temperatures of less than 10 K, the emission first exhibits a redshift with increasing temperature. This redshift is produced by thermally activated occupation of deeper localized states. With further increasing temperature the occupation of delocalized states gains increasing influence, and the emission maximum shifts to higher photon energies. Above moderate temperatures of ~100 K this blueshift is counterbalanced by a temperature-induced band-gap reduction which is insignificant for low temperatures.[27] This *s*-type behavior of the spectral position of the emission maximum is characteristic of disordered systems.

In the case of the *s* sample, temperature-dependent μ-PL measurements clearly demonstrate thermally activated redistribution processes (see Fig. 2). Since the structural correlation length of this sample is significantly shorter than the exciton Bohr radius, localization effects are not much more pronounced than, for example, in a disordered semiconductor alloy. The μ-PL spectra at low temperatures are therefore almost smooth, indicating that the main contributions to the PL stem from delocalized or nearly delocalized states. However, a temperature increase up to about 40 K leads to a drastic change of the μ-PL properties. On the low-energy side, sharp emission lines corresponding to single-exciton states occur. The occupation of these deeper localized states produces a small redshift of the emission maximum and a significant broadening of the envelope PL line. A further increase of temperature favors the occupation of delocalized states and the emission maximum shifts to higher photon

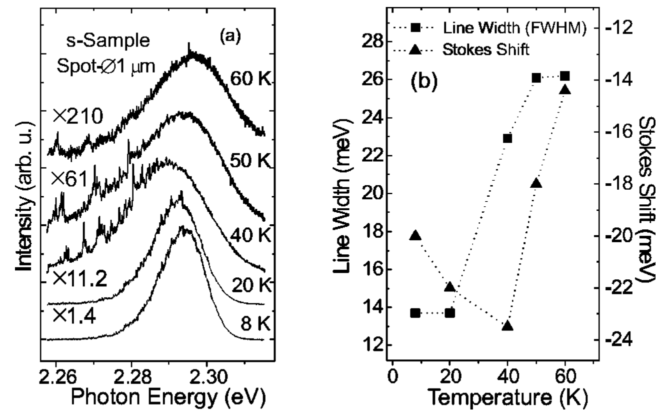

FIG. 2. (a) Normalized μ-PL spectra of the *s* sample recorded for different temperatures. The normalization factors are given with respect to the 8-K spectrum. (b) Linewidth [full width at half maximum (FWHM)] and Stokes shift of the envelope emission line as functions of lattice temperature. The zero Stokes shift corresponds to the absorption resonance determined by PLE at low temperature (not shown). The temperature dependence of the band gap was extracted from single trackable lines in the μ-PL spectra.

energies. At 60 K most of all excitons are delocalized, and only the deepest sharp lines remain. Due to the increasing importance of nonradiative recombination, which is caused by the increased exciton mobility, the quantum efficiency decreases significantly [see the normalization factors in Fig. 2(a)].

Since the structural correlation length of the *l* sample is comparable to the exciton Bohr radius, localization effects have a much more pronounced influence on the optical properties of this sample. For example, low-temperature μ-PL spectra recorded at $T=5$ K are characterized by narrow lines which occur over the whole energy range of the emission (see Fig. 7). Furthermore, the examination of the spatially integrated PL yields that both linewidth and Stokes shift are much larger than in the case of the *s* sample. In order to determine the band-gap energy, we performed photoluminescence excitation (PLE) measurements at low temperatures. The temperature dependence of the band gap was extracted by the temperature induced shift of single trackable lines in the temperature-dependent μ-PL experiments. However, this procedure works only up to temperatures of ~80 K, since the low quantum efficiency requires integration times that are too long. In order to determine the band-gap at higher temperatures, we have used the spectral dependence of the optical anisotropy. This is described in Sec. V A.

The *s*-type dependence of the PL maximum position on temperature is clearly discernible in Fig. 3. Above 100 K the redshift is produced by the temperature dependence of the band gap. As for the *s* sample, the nonmonotonous behavior for lower temperatures is the result of thermally activated redistribution processes. However, a closer examination of the line parameters (see Figs. 2 and 3) yields an important difference between the two samples. While for the *s* sample the linewidth increases monotonically over the whole temperature range, i.e., in particular above the temperature which is sufficient for the occupation of delocalized states, the linewidth of the *l* sample exhibits a local maximum at 100 K. The line shape at this temperature indicates that the

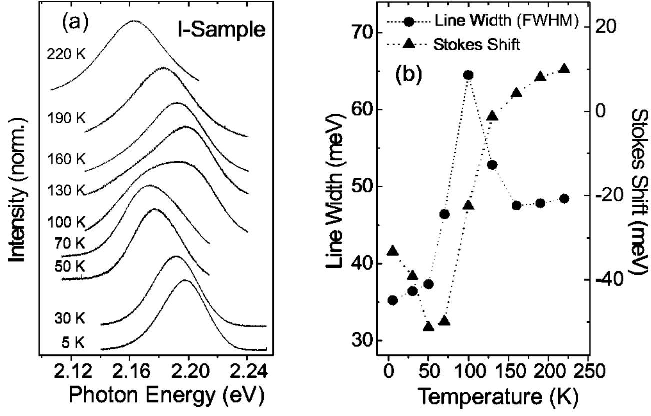

FIG. 3. (a) PL spectra of the l sample recorded for different temperatures. (b) Linewidth (FWHM) and Stokes shift as functions of temperature. Below 80 K the Stokes shift was determined by μ-PL as in the case of the s sample. Above 80 K the band-gap energy was obtained by the maximum of the anisotropy.

emission is composed of at least two separated contributions. This is a first indication for the existence of two different types of localized states in this particular nanostructure, i.e., a lower-energy type and a higher-energy type. In Sec. V we show that the ordering-induced anisotropy is modified as a consequence of contributions from the lower-energy type of localized states.

V. SPECTRAL DEPENDENCE OF THE OPTICAL ANISOTROPY

In Sec. IV we demonstrated that the optical properties of the l sample are strongly modified by localization effects. In order to investigate the influence of localization which results from the particular *nanostructure* on the ordering-induced anisotropy, which is a consequence of a CuPt$_B$-type *crystal structure*, we have determined the spectral dependence of the optical anisotropy.

As a consequence of the lower symmetry of ordered crystals, the fundamental optical transition between the Γ_6^C conduction-band and $\Gamma_{4,5}^V$ valence-band states is forbidden for light polarization parallel to the ordering direction. For light emission along [001] (corresponding to the usual geometry of a PL experiment), [110] (X) and $[\bar{1}10]$ (Y) are the polarization directions of maximum and minimum intensity, respectively. In the following the ratio I_X/I_Y between maximum and minimum intensity is denoted as anisotropy A.

If there is no epitaxial strain, the above mentioned selection rule yields the value $A=3$ for transitions at $\mathbf{k}=0$.[9] These optical transitions correspond to one particular photon energy equal to the fundamental band-gap energy E^0. For higher-energy transitions, i.e., transitions with nonzero momentum $\mathbf{k}$, the optical anisotropy is modified as a consequence of the complicated structure of the upper valence band Γ_8^V in a disordered system. These modifications are discussed in Sec. V A.

As mentioned above, the low-energy localized states produce additional modifications of the optical anisotropy. These modifications on the low-energy side of the spectra are discussed in Sec. V B. In Sec. V C we compare the spectral dependence of the anisotropy which was obtained experimentally with the theoretical considerations of Sec. V A and V B.

A. High-energy side: effect of band mixing

With increasing temperature the occupation of higher energy states with $\mathbf{k}\neq 0$ gains increasing influence. For optical transitions between conduction- and valence-band states with $\mathbf{k}\neq 0$, the anisotropy depends on $\mathbf{k}$ and thus deviates from the value of 3. This is a consequence of valence-band mixing. In order to investigate the $\mathbf{k}$ dependence of A, we consider ordering as chemical strain as done by Wei and Zunger,[9] and assume that the degree of ordering is not too high. Then one can neglect the coupling between the upper valence band Γ_8^V and the split-off band Γ_7^V which is split due to spin-orbit interaction. In this case the ordering-induced valence-band splitting $\Delta_{\mathrm{lh}}(0)$ at the Γ point is given by[11]

$$\Delta_{lh}(0)=2\sqrt{3}|d_v\epsilon_{xy}|, \tag{1}$$

where ϵ_{xy} is the off-diagonal element of the strain tensor, and d_v stands for the hole deformation potential. In the following we ignore exciton effects, and calculate the probabilities of the interband optical transitions which are defined by the matrix elements of the electron-photon interaction Hamiltonian

$$W_{i\mathbf{e}}=|\langle\psi_c|\mathbf{e}\hat{\mathbf{p}}|\psi_{iv}\rangle|^2. \tag{2}$$

In Eq. (2), $\hat{\mathbf{p}}$ is the momentum operator, and $\mathbf{e}$ is the polarization vector; the wave functions ψ_c and ψ_{iv} refer to the conduction band Γ_6^C and the valence band Γ_8^V; and $i=l,h$ denotes light and heavy holes, respectively. The electron wave functions ψ_c have s-like symmetry, and are defined by the spin functions $\psi_c=|S\rangle\alpha,|S\rangle\beta$. For nonzero momentum $\mathbf{k}$ as well as in the presence of deformations, the hole wave functions ψ_{iv} are linear combinations of the basis functions $|\mathbf{J},i_z\rangle$, with $\mathbf{k}$- and strain-dependent coefficients.[28] One can check, in particular, that for $[1\bar{1}1]$ or $[\bar{1}11]$ strain, the hole wave functions are given by

$$\psi_{iv}=B_i\left[H\left|\frac{3}{2},\frac{3}{2}\right\rangle\mp[G-\Delta_{\mathrm{lh}}(\mathbf{k})]\left|\frac{3}{2},\frac{1}{2}\right\rangle+I\left|\frac{3}{2},-\frac{3}{2}\right\rangle\right]. \tag{3}$$

With the Luttinger parameters $\gamma_{2,3}$, the coefficients H, G, and I are given by

$$H=2\sqrt{3}\gamma_3k_z(k_y+ik_x)+d_v\epsilon_{xy}(1-i),$$

$$G=-2\gamma_2\left[k_z^2-\frac{1}{2}(k_x^2+k_y^2)\right],$$

$$I=\sqrt{3}[-\gamma_2(k_x^2-k_y^2-2ik_xk_y)]+id_v\epsilon_{xy}, \tag{4}$$

the $\mathbf{k}$-dependent valence-band splitting is

$$\Delta_{\mathrm{lh}}(\mathbf{k})=2\sqrt{G^2+|H|^2+|I|^2}, \tag{5}$$

and for the coefficients B_i we obtain

$$B_i=[2(\Delta_{\mathrm{lh}}(\mathbf{k})\mp G)\Delta_{\mathrm{lh}}(\mathbf{k})]^{1/2}. \tag{6}$$

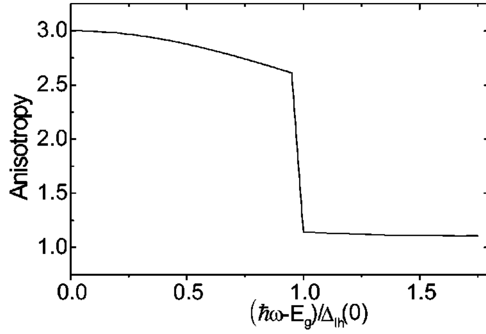

FIG. 4. Calculated anisotropy as a function of kinetic energy. The valence-band splitting at the Γ point is denoted as $\Delta_{\rm lh}(0)$, and E_g is the band-gap energy. The reduced mass is $\mu = 0.07$, and the Luttinger constant is $\gamma_2 = 1$.

In Eqs. (3) and (6) the upper sign corresponds to the heavy-hole states and the lower one to the light-hole states, if the product $d_v \epsilon_{xy} < 0$ as assumed for CuPt$_B$-type ordered $(Al_xGa_{1-x})_{0.52}In_{0.48}P$ crystals.

The transition probabilities [Eq. (2)] calculated with functions (3)–(6) are **k** dependent. This dependence can be converted into an energy dependence using the momentum and energy conservation law. In the spherical approximation $\gamma_2 = \gamma_3$, averaging over all values of **k** reduces to averaging over all directions of **k**. When the photon energy is smaller than $E_g + \Delta_{\rm lh}(0)$, only transitions into heavy-hole states are possible. In this case the optical anisotropy, which is identified by the ratio of the probabilities W_X and W_Y, is given by $A(\hbar\omega) = W_X(\hbar\omega)/W_Y(\hbar\omega)$. For higher photon energies there are additional transitions into light-hole states, and we obtain

$$A(\hbar\omega) = \frac{W_{hX}(\hbar\omega) + W_{lX}(\hbar\omega)}{W_{hY}(\hbar\omega) + W_{lY}(\hbar\omega)}. \tag{7}$$

The result of this calculation is depicted in Fig. 4. We have performed the calculation with the values $\mu = 0.07$ and $\gamma_2 = 1$ for the reduced mass and the Luttinger parameter, respectively. These values are typical for $Ga_{0.52}In_{0.48}P$,[29] though the exact values for $(Al_{0.5}Ga_{0.5})_{0.52}In_{0.48}P$ are not known. Starting from the value 3 at $k = 0$ the anisotropy decreases monotonically with increasing (kinetic) energy. At the energy $E_0 = E_g + \Delta_{\rm lh}(0)$, contributions from light-hole transitions lead to an abrupt decrease to values close to 1. Similar results have previously been found by Bir and Ivchenko,[30] but in the case of hexagonal crystals.

B. Low-energy side: effect of localization

Localized states can be considered as local potential minima for excitons. In the following we show that emission from these minima is anisotropic if their geometrical shape is nonspherical. Therefore we call these potential minima anisotropic localization centers (ALC's). As a simple model we consider quasi-zero-dimensional centers (quantum dots), and discuss the influence of the nonspherical shape on the optical anisotropy. For other materials, polarized emission from nonspherical localization centers (quantum dots) were observed experimentally.[31–33] CuPt$_B$-type ordering is neglected in this section. Actually, this is justified since the contribution of ordering to the anisotropy is exceeded by the effect of the ALC's. This will be shown in Sec. V C.

In Ref. 34 nonstrained single quantum dots of elliptical shape, with the main axes along the main cubic axes {100}, were considered. The confinement was modeled via a harmonic potential with three different eigenfrequencies ω_x, ω_y, and ω_z. Then the effective-mass Hamiltonian for the electron is a three-dimensional harmonic oscillator, and the wave functions are defined by the three quantum numbers N_y, N_y, and N_z. The hole Hamiltonian can be written in the form $H_{\Gamma_8} = H_s + H_c$, where the terms H_s and H_c represent the spherical and cubic parts, respectively. In the spherical approximation, the eigenvalues of H_s are similar to those for the electron. However, each hole state with a given set of quantum numbers is fourfold degenerate. The nonspherical part of the Luttinger Hamiltonian, H_c, breaks this degeneracy. Both states with equal quantum numbers and states with different quantum numbers are mixed by the interaction part H_c. If the ellipticity of the quantum dot is small, the effect of H_c can be calculated using the Löwdin method.[35] Then, the interaction of the degenerate states is included exactly, and the interaction of the states with different eigenvalues is treated as a perturbation.

Herein we consider nonspherical quantum dots whose main axes are oriented along [110] (X), [$\bar{1}$10] (Y), and [001] (Z). The lengths of the cross-sectional axes are denoted as L_i ($i = X,Y,Z$) and the nonspherical shape is described by the ratios $\alpha = (L_X/L_Y)^2$ and $\beta = (L_X/L_Z)^2$. We focus our attention on the optical transitions from the uppermost valence-band state to the lowest conduction-band state with $\{N_x, N_y, N_z\} = 0$.

As an example we consider a quantum dot which is slightly elongated along the [$\bar{1}$10] direction, i.e., $\alpha < 1$ and $\alpha < \beta$. One can show that in this case the Bloch part of the wave function of the uppermost valence band state is the following linear combination of the basis states $|\mathbf{J}, j_z\rangle$,

$$\psi_v = \frac{1}{N}\left[(Q+\delta)\left|\frac{3}{2},\frac{3}{2}\right\rangle + M\left|\frac{3}{2},-\frac{1}{2}\right\rangle \right], \tag{8}$$

where

$$\delta = \sqrt{Q^2 + M^2}, \quad N = 2\sqrt{\delta(\delta + Q)}, \tag{9}$$

and the coefficients Q and M are given by

$$Q = \gamma_2(2\beta - \alpha - 1), \quad M = \sqrt{3}\gamma_3(1-\alpha). \tag{10}$$

For the transition probabilities which are given by Eq. (2), we obtain

$$W_X = \frac{|P|^2}{3}\left[1 + \frac{(2\beta - 1 - \alpha) - 3\dfrac{\gamma_2}{\gamma_3}(1-\alpha)}{2\tilde{\delta}} \right], \tag{11}$$

$$W_Y = \frac{|P|^2}{3}\left[1 + \frac{(2\beta - 1 - \alpha) + 3\dfrac{\gamma_2}{\gamma_3}(1-\alpha)}{2\tilde{\delta}} \right],$$

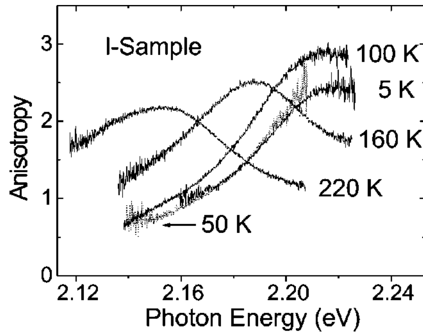

FIG. 5. Spectral dependence of the anisotropy obtained by polarized PL (l sample) for different temperatures.

$$W_Z=\frac{|P|^2}{3}\left[1-\frac{(2\beta-1-\alpha)}{\tilde{\delta}}\right].$$

The ratio γ_2/γ_3 describes the degree of warping for the Γ_{8v} valence band, and

$$\tilde{\delta}=\sqrt{(2\beta-1-\alpha)^2+3\left(\frac{\gamma_2}{\gamma_3}\right)^2(1-\alpha)^2}. \tag{12}$$

Evidently, the transition probabilities depend only on the axis ratios. The results above are similar to those obtained in Ref. 34. However, due to the change of the quantum-dot orientation, the warping factor appears in Eq. (11). Usually, the warping effect is small, and the ratio γ_2/γ_3 is close to 1. For example, in the case of InP crystals, the Luttinger parameters are $\gamma_2=1.6$ and $\gamma_3=1.7$–2.3.[29] This yields a warping factor of $\simeq 1.07$–1.4. It is important to note that, according to Eq. (11), the warping is not the reason for the considered anisotropy, but only the nonspherical shape. Actually, for $\alpha=1$, Eq. (11) yields equal probabilities $W_X=W_Y$.

If we take, for simplicity, the spherical approximation $\gamma_2\simeq\gamma_3$ and assume that $\beta\simeq 1$, we obtain

$$W_Y=\frac{2}{3}|P|^2, \quad W_X=\frac{|P|^2}{6}, \tag{13}$$

i.e., a (small) elongation along $[\bar{1}10]$ produces a strong anisotropy $A=W_X/W_Y=0.25$. Note that A is smaller than 1 in this particular case, while it is always larger than 1 in the case of CuPt$_B$-type ordering.

C. Experimental results

For some selected spectra of Fig. 3 the corresponding spectral dependence of the anisotropy A is depicted in Fig. 5. For $T=5$ K, A increases monotonically with increasing photon energy, and reaches its maximum value of ~ 2.5 on the high-energy end of the emission line. This value is close to the theoretical value of 3. Unlike the corresponding emission line [see Fig. 3(a)], the anisotropy spectrum remains almost constant if the temperature is increased up to 50 K. Hence the origin of the redshift of the emission is unambiguously attributed to a thermally activated exciton redistribution within the same type of localized states. The main difference between the 5 K and 50-K anisotropy spectra can be found on the low-energy end, where the anisotropy at 50 K is significantly smaller than 1. This stands definitely in contradiction to the ordering-induced anisotropy, i.e., for the deepest states CuPt$_B$-type ordering is not the origin of the anisotropy.

We explain this experimental result by the existence of ALC's. Deeply localized centers in ordered $Ga_{0.52}In_{0.48}P$ (often called quantum dots) were reported by Kops *et al.*[19] Kops *et al.* attributed these quantum dots to In-rich clusters occurring at the antiphase boundaries. In the present case the ALC's may be correlated to In-rich clusters which occur in the particular nanostructure of the l sample. Since they do not occur in the s sample, we conclude that the formation of these clusters requires a minimum domain size. As described in Sec. V B, a small elongation of the potential minima along $[\bar{1}10]$ is sufficient to produce the observed anisotropy.

In the particular nanostructure of the l sample, we have at least two types of localized states. Anisotropic localization centers which may be correlated to In-rich clusters dominate the low-energy end of the emission. On the high-energy end at low temperatures, the anisotropy is consistent with ordering. In this energy range localization is caused by fluctuations of the degree of ordering. We explain the spectral dependence of A at lower temperatures by the coexistence of ordering and clustering in this particular nanostructure. Furthermore, this coexistence explains the temperature dependence of the linewidth which was mentioned above. At 100 K the contributions of clusters and ordering-related localized states are comparable, and thus the linewidth exhibits a local maximum. For lower temperatures ALC's dominate, and above 100 K ordering-related states are more important.

With increasing temperature the exciton mobility increases, i.e., excitons become delocalized and thus free states with $k\neq 0$ contribute to the PL. As expected, the anisotropy decreases with increasing photon energy. However, the abrupt jump at E_0 predicted by the calculation described above (see Fig. 4) has not been observed in experiment, since the band gap and thus the value of E_0 exhibit spatial fluctuations. If we compare the anisotropy spectra for 160 and 220 K, two main features become obvious. On the one hand, ALC-related recombination loses importance. While at 160 K the anisotropy on the low-energy end approaches 1, A does not fall far below the value of 2 at 220 K. On the other hand, the contribution of light-hole states gains increasing importance. Therefore, the anisotropy disappears, i.e., approaches 1 on the high-energy end for 220 K, but not yet for 160 K. In addition, light-hole contributions are responsible for the decrease of the maximum anisotropy with temperature.

Above 100 K the spectral dependence of A is nonmonotonic, exhibiting a local maximum. This maximum separates localized from extended states, and its spectral position is therefore attributed to the mobility edge which can be assumed to be the fundamental band edge of the localized system. Hence, for temperatures above 100 K (see Fig. 3), we have defined the Stokes shift as the energy difference between the emission maximum and anisotropy maximum. The delocalization and increasing occupation of higher-energy states including light-hole states is reflected by the positive sign of the Stokes shift above 100 K (see Fig. 3).

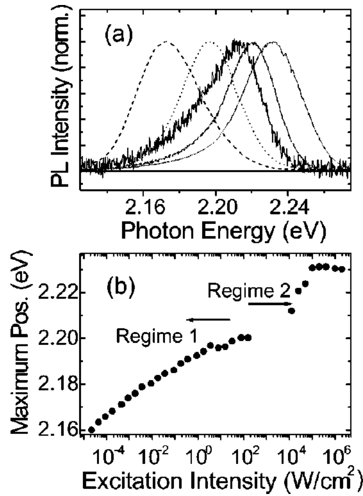

FIG. 6. (a) PL spectra of the l sample recorded for different excitation intensities: 0.4 mW/cm^2 (dashed line); 3.5 W/cm^2 (dotted line); and 12.5, 25, and 400 kW/cm^2 (solid line). (b) PL maximum position as a function of excitation intensity.

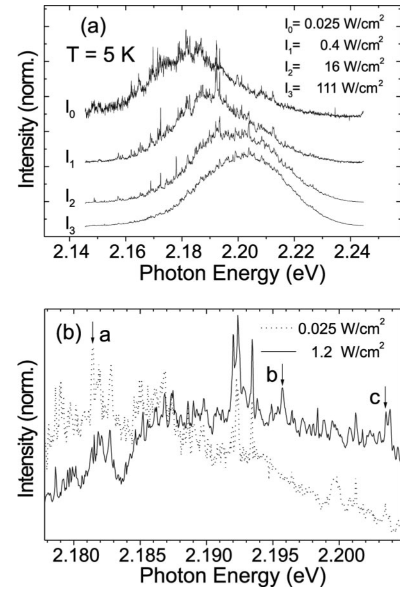

FIG. 7. (a) μ-PL spectra of the l sample recorded for different excitation intensities. (b) Parts of the μ-PL spectra for two different excitation intensities. The blueshift of the total emission is not caused by a blueshift of single lines. With increasing intensity, lines on the low-energy side decrease (a). On the high-energy side, additional lines pop up (b), or existing lines increase (c).

VI. STATE FILLING

With increasing excitation intensity both samples exhibit a blueshift of the emission. While this effect is weak for the s sample, it is very pronounced in the case of the l sample. Figure 6 shows PL spectra for different excitation intensities. If we look at the spectral position of the emission maximum as a function of excitation intensity, we can distinguish between two excitation regimes (see Fig. 6). The blueshift in the low-intensity regime saturates for several hundred kW/cm^2. In the high-intensity regime above 10 kW/cm^2, an initial strong blueshift is followed by saturation at ~ 100 kW/cm^2. In the following we show that state filling is the origin of the blueshift. This filling takes place in two steps. We discuss these two steps corresponding to the two excitation regimes separately.

A. Low intensities: Local filling and moving emission

For ordered $Ga_{0.52}In_{0.48}P$ it was reported very frequently that the low-energy emission exhibits a characteristic blueshift with increasing excitation intensity.[16,36,37] This phenomenon was sometimes called *moving emission*. It was suggested that internal electric fields are the reason for this behavior. In particular, ordering-induced piezoelectric fields, in combination with a fluctuating potential which is caused by the inhomogeneous microstructure (nanostructure) lead to a spatial separation of electrons and holes. As a consequence, the emission is redshifted (quantum-confined Stark effect[38]), and the decay times are very long. With increasing excitation intensity screening of the internal fields leads to an attenuation of the quantum-confined Stark effect, and thus to a blueshift of the emission.

Microphotoluminescence is a convenient method to check this proposal. If this was correct, one should observe single lines which shift to the blue with increasing excitation intensity, since these lines correspond to single localized states which shift to higher energies as a consequence of screening. However, we have not found any single line which exhibits this behavior. In Fig. 7(a) μ-PL spectra for different excitation intensities are depicted. As can be seen very clearly in Fig. 7(b), the lines on the low-energy side decrease with increasing excitation, while the lines on the high-energy side gain increasing importance.

Therefore, we can exclude the screening of internal fields as origin of the moving emission. We attribute the blueshift to a local state filling including the occupation of excited states in each anisotropic localization center. However, the thermal redistribution described above has been observed for all intensities in this low-excitation regime, i.e., there is no global state filling for these intensities.

B. High intensities: Global state filling

In contrast to the low-intensity regime, a closer examination of the spectra in the high-excitation regime yields that the line shape remains almost constant when the intensity is increased.[39] In this regime we assume that the ALC's are saturated, and that filling of shallower ordering-related localized states takes place. This global filling prevents any thermal redistribution. As shown in Fig. 8, no thermally activated redshift is observed for an intensity of 900 kW/cm^2. A further increase of the optical pump power leads to the occurence of stimulated emission.[39]

VII. SUMMARY

Using photoluminescence (PL), microphotoluminescence (μ-PL), and high-excitation spectroscopy we have investigated the influence of localization on the optical properties of ordered $(Al_{0.5}Ga_{0.5})_{0.52}In_{0.48}P$. Localization is caused by potential fluctuations which occur in inhomogeneous microstructures (nanostructures). Such structures are always formed in $CuPt_B$-ordered crystals. The significance of localization effects depends strongly on the particular type of mi-

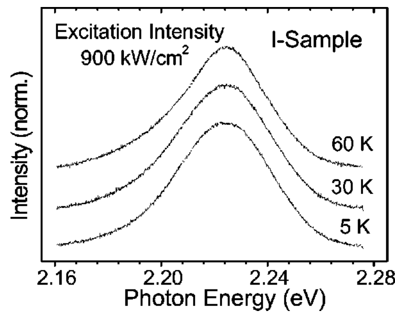

FIG. 8. PL spectra of the *l* sample recorded at 900 kW/cm^2. The emission remains almost constant with increasing temperature, since thermally activated redistribution is blocked (global state filling).

crostructure (nanostructure), especially on the structural correlation length. In order to verify this we have compared two samples which were grown simultaneously, but on differently oriented substrates. As a consequence of the substrate orientation, the nanostructures of the samples are completely different. One sample exhibits very pronounced localization effects, and the other shows only weak modifications of the optical properties.

For both samples we have found thermally activated exciton redistribution in temperature-dependent PL and μ-PL experiments. The thermally activated occupation of deeply localized states at moderate temperature is followed by the occupation of extended states at higher temperatures. As a consequence, the position of the emission maximum exhibits an *s*-type behavior for increasing temperature.

For the sample with strong localization effects, the ordering-induced anisotropy is modified by localization. In particular, the polarization of the emission from the deepest localized states is not affected by ordering. These states occur as anisotropic localization centers and may be correlated to nonspherical In-rich clusters which are present in this particular nanostructure. The anisotropic localization centers dominate the emission for low temperatures and low-excitation intensities.

In addition, we have calculated the anisotropy of transitions from higher-energy extended states which are occupied for high temperatures. We have found that the maximum anisotropy of the [001] emission is located at the mobility edge. For temperatures above 100 K we can therefore determine the mobility edge energy by measuring the spectral dependence of the optical anisotropy.

With increasing excitation intensity localized states are filled. This process evolves in two steps. At lower intensities the clusters are filled, and excited, cluster-related, states are occupied. This local state filling leads to a blueshift of the emission which saturates for moderate intensities of several hundreds of kW/cm^2. Further increasing the intensity results in a global state filling connected with a strong blueshift with increasing intensity. In this intensity range thermally activated redistribution processes are blocked.

ACKNOWLEDGMENTS

We wish to thank D. J. Mowbray and C. C. Button for fruitful cooperation. In addition, we thank E. Weckert, S. Ginder, W. Send, and D. Gerthsen for the characterization of the samples which has been performed by x-ray diffraction and transmission electron microscopy. This work was supported by the Deutsche Forschungsgemeinschaft.

*Permanent address: Institute for Cybernetics, Academy of Sciences, S. Euli 5, 380086 Tbilisi, Georgian Republic.

[1] R. Zimmermann, J. Cryst. Growth **101**, 346 (1990).

[2] S.D. Baranovskii, U. Doerr, P. Thomas, A. Naumov, and W. Gebhardt, Solid State Commun. **89**, 5 (1994).

[3] F. Yang, M. Wilkinson, E.J. Austin, and K.P. O'Donnell, Phys. Rev. Lett. **70**, 323 (1993).

[4] S.K. Lyo, Phys. Rev. B **48**, 2152 (1993).

[5] G.P. Srivastava, J.L. Martins, and A. Zunger, Phys. Rev. B **31**, 2561 (1985).

[6] A. Gomyo, T. Suzuki, K. Kobayashi, and I. Hino, Appl. Phys. Lett. **50**, 673 (1987).

[7] A. Gomyo, T. Suzuki, and S. Iijima, Phys. Rev. Lett. **60**, 2645 (1988).

[8] T. Suzuki, A. Gomyo, and S. Iijima, J. Cryst. Growth **93**, 396 (1988).

[9] S.-H. Wei and A. Zunger, Phys. Rev. B **49**, 14 337 (1994).

[10] S.-H. Wei and A. Zunger, Phys. Rev. B **57**, 8983 (1998).

[11] E.G. Tsitsishvili, Phys. Rev. B **59**, 10 044 (1999).

[12] G.S. Chen and G.B. Stringfellow, Appl. Phys. Lett. **59**, 324 (1991).

[13] P. Bellon, J.P. Chevalier, E. Augarde, J.P. André, and G.P. Martin, J. Appl. Phys. **112**, 2388 (1989).

[14] T. Suzuki, A. Gomyo, and S. Iijima, J. Cryst. Growth **99**, 60 (1990).

[15] S. Smith, H.M. Cheong, B.D. Fluegel, J.F. Geisz, J.M. Olson, L.L. Kazmerski, and A. Mascarenhas, Appl. Phys. Lett. **74**, 706 (1999).

[16] P. Ernst, C. Geng, G. Hahn, F. Scholz, H. Schweizer, F. Phillipp, and A. Mascarenhas, J. Appl. Phys. **79**, 2633 (1996).

[17] U. Kops, R.G. Ulrich, M. Burkard, C. Geng, F. Scholz, and M. Schweizer, Phys. Status Solidi A **164**, 459 (1997).

[18] H.M. Cheong, A. Mascarenhas, S.P. Ahrenkiel, K.M. Jones, J.F. Geisz, and J.M. Olson, J. Appl. Phys. **83**, 5418 (1998).

[19] U. Kops, P.G. Blome, M. Wenderoth, R.G. Ulrich, C. Geng, and F. Scholz, Phys. Rev. B **61**, 1992 (2000).

[20] U. Dörr, H. Kalt, W. Send, D. Gerthsen, D.-J. Mowbray, and C.C. Button, Appl. Phys. Lett. **73**, 1679 (1998).

[21] O.P. Kowalski, R.M. Wegerer, D.J. Mowbray, M.S. Skolnick, C.C. Button, J.S. Roberts, M. Hopkinson, J.P.R. David, and G. Hill, Appl. Phys. Lett. **68**, 3266 (1996).

[22] D. Lüerßen, A. Oehler, R. Bleher, and H. Kalt, Phys. Rev. B **59**, 15 862 (1999).

[23] S.D. Baranovskii, R. Eichmann, and P. Thomas, Phys. Rev. B **58**, 13 081 (1998).

[24] E. Runge and R. Zimmermann, Adv. Solid State Phys. **38**, 251 (1999).

[25] R. Zimmermann and E. Runge, Phys. Status Solidi A **164**, 511 (1997).

[26] Y.-H. Cho, G.H. Hainer, A.J. Fischer, J.J. Song, S. Keller, U.K. Mishra, and S.P. DenBaars, Appl. Phys. Lett. **73**, 1370 (1998).

[27] D. Lüerßen, R. Bleher, and H. Kalt, Phys. Rev. B **61**, 15 812 (2000).

[28] G.L. Bir and G.E. Pikus, *Symmetry and Strain-Induced Effects in Semiconductors* (Wiley, New York, 1974).
[29] Landolt–Börnstein, *Numerical Data and Functional Relationships in Science and Technology, Semiconductors. Intrinsic Properties of Group IV Elements and III-V, II-VI, and I-VII Compounds*, edited by O. Madelung, Landolt–Börnstein, New Series, Group III, Vol. 22, Pt. a (Springer-Verlag, Berlin, 1990).
[30] G.L. Bir and E.L. Ivchenko, Fiz. Tekh. Poduprovodn **9**, 1300 (1975) [Sov. Phys. Semicond. **9**, 858 (1975)].
[31] Y. Nabetani, T. Ishikawa, S. Noda, and A. Sasaki, J. Appl. Phys. **76**, 347 (1994).
[32] H. Saito, K. Nishi, S. Suguo, and Y. Sujimoto, Appl. Phys. Lett. **71**, 590 (1997).
[33] M. Henini, S. Sanguinetti, S.C. Fortuna, E. Grilli, M. Guzzi, G. Panzarini, L.C. Andreani, M.D. Upward, P. Moriarty, P.H. Beton, and L. Eaves, Phys. Rev. B **57**, R6815 (1998).
[34] E.G. Tsitsishvili, Appl. Phys. A: Mater. Sci. Process. **66**, 189 (1998).
[35] P.O. Löwdin, J. Chem. Phys. **19**, 1396 (1951).
[36] J.E. Fouquet, V.M. Robbins, J. Rosner, and O. Blum, Appl. Phys. Lett. **57**, 1566 (1990).
[37] M.C. Delong, P.C. Taylor, and J.M. Olson, Appl. Phys. Lett. **57**, 620 (1990).
[38] D.A.B. Miller, D.S. Chemla, T.C. Damen, A.C. Gossard, W. Wiegmann, T.H. Wood, and C.A. Burrus, Phys. Rev. Lett. **53**, 2173 (1984).
[39] U. Dörr, H. Kalt, D.J. Mowbray, and C.C. Button, Appl. Phys. Lett. **72**, 821 (1998).